Surface-Induced Orientation Control of CuPc Molecules for the Epitaxial Growth of Highly Ordered Organic Crystals on Graphene

Kai Xiao,*,[†] Wan Deng,[⊥] Jong K. Keum,[‡] Mina Yoon,[†] Ivan V. Vlassiouk,[§] Kendal W. Clark,[†] An-Ping Li,[†] Ivan I. Kravchenko,[†] Gong Gu,[⊥] Edward A. Payzant,[‡] Bobby G. Sumpter,[†] Sean C. Smith,[†] James F. Browning,[‡] and David B. Geohegan[†]

[†]Center for Nanophase Materials Sciences, [‡]Chemical and Engineering Materials Division, and [§]Measurement Science and System Engineering Division, Oak Ridge National Laboratory, Oak Ridge, Tennessee 37831, United States

[⊥]Department of Electrical Engineering and Computer Science, University of Tennessee at Knoxville, Knoxville, Tennessee 37931, United States

Ⓢ *Supporting Information*

ABSTRACT: The epitaxial growth and preferred molecular orientation of copper phthalocyanine (CuPc) molecules on graphene has been systematically investigated and compared with growth on Si substrates, demonstrating the role of surface-mediated interactions in determining molecular orientation. X-ray scattering and diffraction, scanning tunneling microscopy, scanning electron microscopy, and first-principles theoretical calculations were used to show that the nucleation, orientation, and packing of CuPc molecules on films of graphene are fundamentally different compared to those grown on Si substrates. Interfacial dipole interactions induced by charge transfer between CuPc molecules and graphene are shown to epitaxially align the CuPc molecules in a face-on orientation in a series of ordered superstructures. At high temperatures, CuPc molecules lie flat with respect to the graphene substrate to form strip-like CuPc crystals with micrometer sizes containing monocrystalline grains. Such large epitaxial crystals may potentially enable improvement in the device performance of organic thin films, wherein charge transport, exciton diffusion, and dissociation are currently limited by grain size effects and molecular orientation.
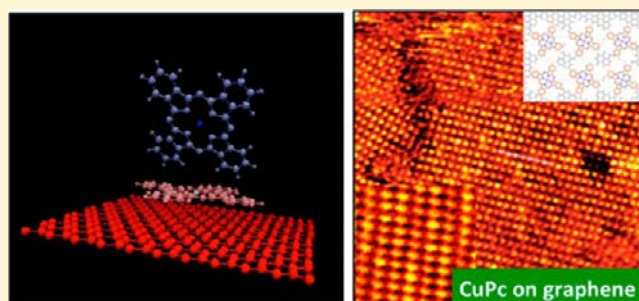
■ INTRODUCTION

Organic π-conjugated molecules are currently being investigated as potential semiconducting components in photovoltaics[1] and field-effect transistors[2] because of their tunable optical and electronic properties.[3] However, a great challenge for the development of high-performance organic semiconductor devices is to arrange the nanoscale morphology and orientation of donor and acceptor phases, as well as the molecules within those phases, in a manner that optimizes the relevant optoelectronic processes required for efficient operation.[4] Details about molecular orientation and packing determine properties such as charge mobility and injection across the interface between the organic materials and electrodes.[5] For organic field-effect transistors (OFETs), the important processes include charge injection and charge transport on both the molecular and device length scales, which are optimized when the π−π stacking direction of the molecules is aligned parallel to the substrate and the conducting channel.[6] For organic photovoltaics (OPVs), however, efficient light absorption, exciton diffusion, and dissociation in thin films rely upon aligning planar molecules face-down to the substrate. In this orientation the transition dipole moment of the planar molecule, which is typically along its long axis, is in alignment

with the electric field of the incident light. The simultaneous optimization of exciton and charge transport relies upon the microstructure and morphology determined by the molecular stacking at both the molecular scale and mesoscale.[7,8] Therefore, it is essential to understand how molecules interact with the substrate to comprise not only the interface in the organic electronic device, but a template to control molecular arrangement at different length scales.

The ordering of organic molecules in films is governed by the interplay between both intermolecular and molecule−substrate interactions.[9] Weak intermolecular interactions in organic thin films allow the molecule−substrate interaction to mediate the molecular orientation and packing, leading to high degrees of order and structural diversity.[10,11] The substrate type and growth temperature have been shown to be important controlling factors for molecular orientation in thin films. In addition, structural templating layers can also be introduced to change the orientation of subsequently adsorbed molecules as an effective way to control molecular orientation, such as face-on or edge-on orientations.[12,13] For example, molecules such as

metal phthalocyanines (Pcs) tend to exhibit an edge-on orientation on the surface of widely used substrates (e.g., SiO$_2$, indium−tin oxide (ITO) or PEDOT/PSS) due to their weak interfacial interaction.[14] This orientation is highly favored in OFETs.[15] However, these molecules have been induced to align in a face-on orientation by inserting a copper iodide (CuI) layer on ITO, which introduced a strong interfacial coupling between the surface electronic states of CuI and the molecular π-orbitals of the CuPc molecules.[16] This face-on orientation of molecules led to an increase in all solar cell parameters, substantially increasing power conversion efficiency from 1.5% to 2.8%.[17] Similarly, organic templating layers such as perylene-3,4,9,10-tertracarboxylic dianhydride (PTCDA)[18] and hexaaza-triphenylene−hexacarbonitrile (HAT-CN)[19] have also been shown to change the orientation of the metal-Pcs, resulting in a preferred face-on orientation of the molecules. However, the devices utilizing these organic templates can have a high-resistance charge injection layer at the anode due to the organic templating layer that blocks hole transport.

Single-layer graphene (SLG) is a semimetal and exhibits mobilities up to 10 000 cm^2/(V s) at room temperature.[20] The multifunctional properties of graphene, including its high conductivity, optical transparency (>95%), and mechanical flexibility, make it widely applicable in optoelectronics.[21] For example, SLG is especially attractive as a transparent conducting electrode (TCE) for organic photovoltaics[22] (as a viable alternative to ITO electrodes[23]) or as an active donor or acceptor in combination with appropriate organic counterparts such as conjugated polymers.[24] Therefore, understanding how graphene can serve both as a TCE and as a template to orient the alignment of organic molecules is crucial for novel solar cell applications. Scanning tunneling microscopy (STM) has proven that a variety of organic molecules (PTCDA, CuPcF$_{16}$, sexiphenyl) form self-assembled monolayers (SAMs) with face-on orientation on epitaxial graphene (grown on both SiC or metal surfaces).[25−29] However, while these studies achieved important milestones, the long-range molecular ordering was essentially isotropic and independent of the underlying graphene lattice. Recently, films of pentacene[30] and NiPc covalent organic frameworks[31] grown on SLG exhibited not only face-on alignment but also long-range structural order. Clearly, there is a need to better understand the interaction between organic molecules and graphene in order to control the alignment and long-range order of crystalline organic thin films for desired optoelectronic properties.

Copper phthalocyanine (CuPc) is a prototypical organic semiconductor that has been commonly used in organic electronics including OFETs[32] and OPVs.[33] CuPc on graphene is an ideal model system to improve the understanding of molecule-surface interactions in graphene-based organic electronics. CuPc molecules adsorbed on metallic substrates and semiconducting surfaces have been widely explored.[34,13,35] Highly ordered pyrolytic graphite was shown using STM and high-resolution electron energy loss spectroscopy (HREELS) to induce order in CuPc molecules to form columnar domains.[36] Recent STM imaging of sub-monolayer films of NiPc and FePc on a substrate of monolayer graphene grown on Ru (0001) was shown to induce interesting periodic "Kagome lattice" supramolecular structure with a variety of interesting patterns.[37] On the other hand, a single layer of graphene on Ni(111) has been shown, using HREELS and Raman spectroscopy, to strongly influence the interaction strength of

different metal-Pcs with the metallic substrate.[38] Thus, graphene on different substrates has been demonstrated to induce a wide variety of morphologies in metal Pcs. However, detailed characterization and understanding of the growth and orientation of CuPc molecules on transferred graphene over the mesoscopic length scales required for organic electronics is lacking.

In this work, we present a combined experimental and theoretical description of the epitaxial growth and preferred orientation of CuPc on graphene. A systematic experimental and theoretical investigation was performed that combined X-ray scattering and diffraction, STM, and scanning electron microscopy (SEM) with first-principles calculations. Both natively grown graphene and graphene transferred onto a Si substrate are shown to act as templates to orient and pack CuPc molecules to a face-on orientation in thin films. In contrast, the edge-on orientation of CuPc is normally induced by surfaces such as oxidized silicon. First-principles theoretical calculations show that the orientation of CuPc molecules on the substrates is determined by the competition between van der Waals (vdW) interactions and an induced dipole interaction via charge transfer with the substrates. Experimental results directly support the theoretical predictions, showing that the nucleation, orientation, and packing of CuPc molecules grown in films on graphene are fundamentally different to films grown on Si substrates. CuPc molecules on a silicon substrate exhibit an edge-on orientation. On the other hand, CuPc is shown to orient in the face-on geometry on graphene for thin films at room temperatures as supported by theory. However, following nucleation into islands and coalescence by edge growth into a continuous thin film CuPc molecules start to tilt up to an edge-on orientation. Higher growth temperatures are able to overcome this orientation change to maintain a fully face-on molecular orientation, forming extremely large, monocrystalline grains of CuPc on graphene within micrometers-size, strip-like crystals. These types of CuPc crystals may potentially enable bulk-like properties for a significant improvement of device properties in organic electronics.

■ RESULTS AND DISCUSSION

In order to obtain information about the out-of-plane ordering of CuPc molecules on various substrates, specular X-ray diffraction (XRD) measurements were conducted (Figure 1). Also, pole figure measurements for (100) and (11$\bar{2}$) reflections
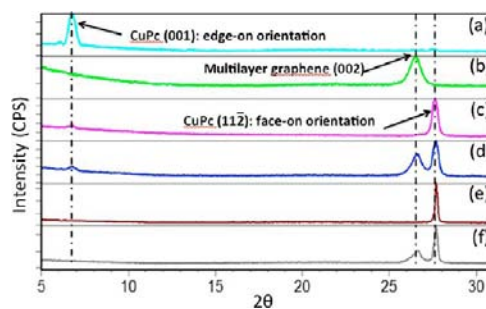

Figure 1. XRD measurements of (a) 20 nm CuPc film grown on silicon substrate with native oxide layer at room temperature, (b) multilayer graphene transferred on Si substrate, (c) 20 nm CuPc film grown on single-layer graphene at room temperature, (d) 20 nm CuPc film grown on multilayer graphene at room temperature, (e) 20 nm CuPc film grown on single-layer graphene at 130 °C, and (f) 20 nm CuPc film grown on multilayer graphene at 130 °C.

of CuPc crystals were performed to probe the global orientation of the CuPc molecules (Figure 2). In the XRD
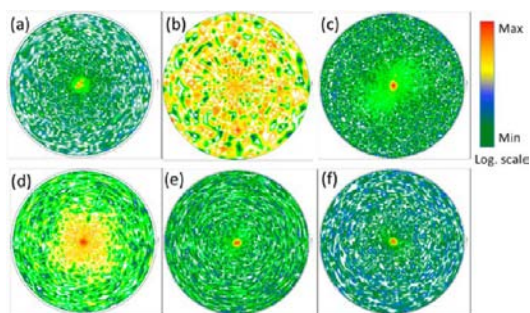

Figure 2. XRD pole figure measurements of CuPc films grown on silicon wafers and graphene. Pole figures measured at (a) $2\theta = 6.83°$ on 20 nm CuPc film on a silicon wafer, (b) $2\theta = 27.68°$ on 20 nm CuPc film on a silicon wafer, (c) $2\theta = 27.68°$ on 20 nm CuPc film grown on graphene at room temperature, (d) $2\theta = 27.68°$ on 50 nm CuPc film grown on graphene at room temperature, (e) $2\theta = 27.68°$ on 20 nm CuPc film grown on graphene at 130 °C, and (f) $2\theta = 27.68°$ on 50 nm CuPc film grown on graphene at 130 °C. Panels (b)−(f) show the measured pole figures for the $(11\bar{2})$ plane of CuPc parallel to the substrate surface. Different intensities represented by different color scales where red areas represent higher intensity. The intensity ranges are (a) 1−211.4, (b) 0.01−2.4, (c) 0.01−71.5, (d) 0.01−66.0, (e) 0.01−292.0, and (f) 0.01−2656.0 cps.

pattern for a CuPc film deposited on a Si substrate with native oxide layer, the most noticeable feature was the Bragg reflection observed at $2\theta = 6.83°$, which was assigned to the α-phase (100).[39] The reflection feature implies that CuPc molecules are oriented perpendicularly to the surface of the Si substrate, i.e., in an edge-on orientation. Pole figures measured at $2\theta = 6.83°$ (Figure 2a) and $2\theta = 27.68°$ (Figure 2b) corroborate such an

orientation, in which the (100) reflections centered at the pole implied that (100) crystal planes were parallel to the surface of the Si substrate. In the $(11\bar{2})$ pole figure measured at $2\theta = 27.68°$, no clear $(11\bar{2})$ maximum was detected, where the total counts at the entire positions were only 0.01−2.4 cps. The $(11\bar{2})$ maximum would exist at around the equator ($\beta = 0$); however, the β range was beyond the detection limit of the X-ray diffractometer used in this study. The aforementioned results based on XRD and pole figure measurements indicate that the (100) planes of CuPc were oriented predominantly parallel to the Si-substrate surface. The molecular orientation with the $\pi-\pi$ packing direction parallel to the substrate is advantageous for enhancing charge transport along that direction and very important for FETs.

For bare graphene transferred onto a Si substrate, SLG does not show any patterns, but the typical (002) peak was observed at $2\theta \approx 26.57°$ from few-layer graphene (FLG, Figure 1b). This could be indexed to an interplanar distance of 3.35 Å, the characteristic (002) plane reflection of graphite.[40] For a 20 nm CuPc film deposited on graphene at room temperature, the XRD pattern appeared totally different. A diffraction peak emerged at $2\theta = 27.68°$, corresponding to an interplanar spacing of 3.22 Å, implying it corresponds to the $(11\bar{2})$ plane of α-phase CuPc (Figure 1c,d). The intensity of the peak at $2\theta = 6.83°$ was significantly lower than that of CuPc film deposited on Si substrate. This indicated that more CuPc molecules adopted a face-on orientation due to the graphene, but still some crystallites adopted the edge-on orientation within the film. In order to study the effect of deposition temperature on the crystal orientation of CuPc, a 20 nm-thick CuPc film was deposited on graphene at 130 °C. No peak was detected at $2\theta = 6.83°$, while the peak at $2\theta = 27.68°$ became much more dominant (Figure 1e,f) as compared to the corresponding peaks when CuPc was deposited at room temperature. This
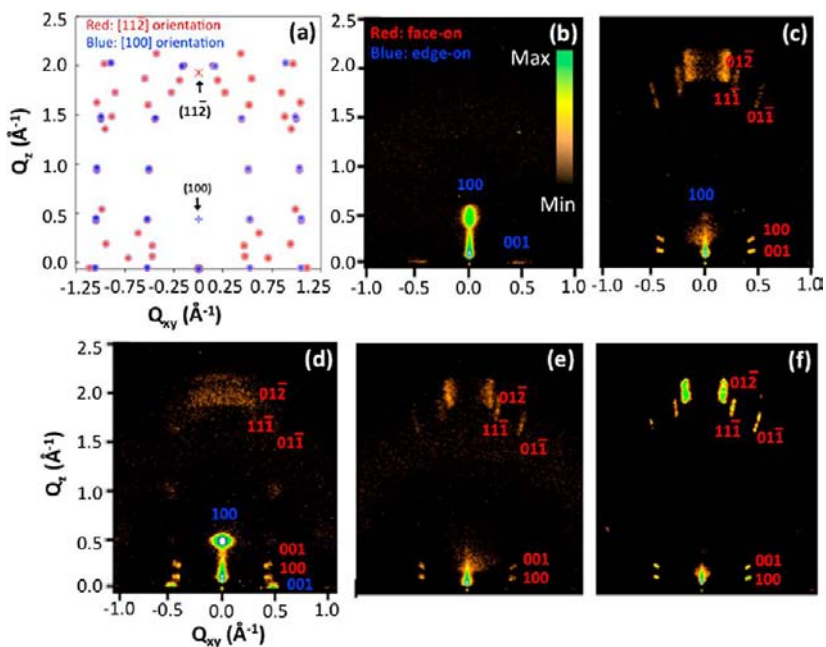

Figure 3. (a) Simulated peak positions for the $[11\bar{2}]$-oriented (red symbols) and [100]-oriented (blue symbols) brickstone structure of α-phase CuPc. (b) GIXD pattern of 20-nm-thick CuPc film on a silicon substrate. (c,d) GIXD patterns for CuPc films grown on graphene at room temperature with thicknesses of (c) 20 and (d) 50 nm. (e,f) GIXD patterns for CuPc films grown on graphene at 130 °C with thicknesses of (e) 20 and (f) 50 nm. The main peaks of interest are indexed for the $(11\bar{2})$-oriented (red symbols) and (100)-oriented (blue symbols) brickstone structure of α-phase CuPc.

suggests that all the crystallites adopted a face-on orientation on graphene. In order to clarify the aforementioned argument, the $(11\bar{2})$ pole figures were measured and are shown in Figure 2c,d. The $(11\bar{2})$ pole figures measured at $2\theta = 27.68°$ for 20 nm-thick CuPc films formed on graphene at room temperature confirm that the $(11\bar{2})$ plane is mainly parallel to the substrate with a moderate orientation distribution (Figure 2c). For the 50 nm-thick CuPc film formed at room temperature, the $(11\bar{2})$ pole figure exhibits reflection maxima at the polar region with a broad distribution (Figure 2d). In contrast, for 20 and 50 nm-thick CuPc films grown on graphene at 130 °C, both of the $(11\bar{2})$ pole figures exhibited much sharper reflection maxima at the polar region (Figure 2e,f) as compared to those of CuPc films deposited at room temperature. A comparison of the reflection intensity and intensity distributions between the pole figures confirms that high temperature growth induces improved crystalline orientation of molecules aligned parallel to the graphene surface.

To further examine the molecular orientation of CuPc, two-dimensional grazing incidence X-ray scattering (2D GIXS) patterns for the same films were collected, and these are depicted in Figure 3b–f. The experimental results were compared with the calculated diffraction patterns corresponding to the crystals with $[11\bar{2}]$ and $[010]$ orientations as shown in Figure 3a. The calculation was based on the brickstone structure CuPc crystal; a triclinic crystal lattice with the lattice parameters, $a = 12.868$ Å, $b = 3.769$ Å, $c = 12.061$ Å, $\alpha = 96.22°$, $\beta = 90.62°$, $\gamma = 90.32°$.[39−42] From the comparison between the calculated and experimental pattern in Figure 3a,b, it can be noticed that, on Si-substrates, CuPc molecules are stacked with their (100) plane parallel to the surface of the Si substrate. Since (100) crystal planes are predominantly parallel to the surface of the Si substrate, a strong (100) diffraction maximum is detected in the vertical direction. On the other hand, the (001) peaks detected in the horizontal direction indicate that the molecular planes of CuPc are aligned perpendicular to the substrate surface in the crystals, as demonstrated in Figure 4a. In contrast, 20 nm-thick CuPc films grown on graphene at room temperature exhibited totally different scattering features as shown in Figure 3c. It is noted that the observed reflection spots coincided with the positions of calculated patterns with a $[11\bar{2}]$ orientation, implying that

CuPc molecules were stacked on graphene in a face-on arrangement. In the case of 50 nm-thick CuPc films prepared on graphene at room temperature, the GIXS patterns is essentially identical to that of the 20 nm-thick CuPc film deposited at room temperature. However, the faint but visible (100) reflection appears in the vertical direction indicating that some portions of crystallites adopted the edge-on orientation, shown in Figure 3c. This suggests a gradual increase in the edge-on molecular arrangements on graphene as the film thickness increases, as demonstrated in Figure 4b. As the 20- and 50-nm-thick CuPc films were prepared on the surface of graphene at high temperature (130 °C), the (100) reflection was not observed in the vertical direction but in the off-axes reflection patterns. The absence of the (100) reflection in the vertical direction implies that at 130 °C, only CuPc crystals with face-on orientation grow on graphene, as demonstrated in Figure 4c. These results are consistent with the aforementioned arguments based on the XRD and pole figure results. It is well known that face-on CuPc crystals grow on PTCDA, HAT-CN, and CuI templates. In the current report we emphasize that a single layer of highly conductive carbon atoms, i.e., SLG, can drive the preferential face-on orientation of a CuPc crystal, critical to out-of-plane charge transport.

Next, we investigate the origin of the molecular orientation of CuPc molecules on graphene using first-principles calculations. Individual CuPc molecules were introduced on graphene in both face-on and edge-on orientation to understand low molecular coverage conditions, where intermolecular (molecule−molecule) interactions are negligible. The CuPc molecule on graphene gains a significant amount of energy in the face-on configuration. The CuPc binding energy to graphene is 3.37 eV. If vdW contributions are not considered, the binding becomes negligible, 0.1 eV on graphene, meaning that vdW plays an important role in stabilizing the configuration. There is also a small amount of charge transfer between the CuPc and graphene. CuPc molecules on graphene are slightly negatively charged with <0.1e, which creates induced dipole moments. However, those effects are still too small to change the CuPc structure significantly, and it remains flat on graphene. The optimized face-on configurations are shown in Figure 5a,b. On the other hand, such a molecule-
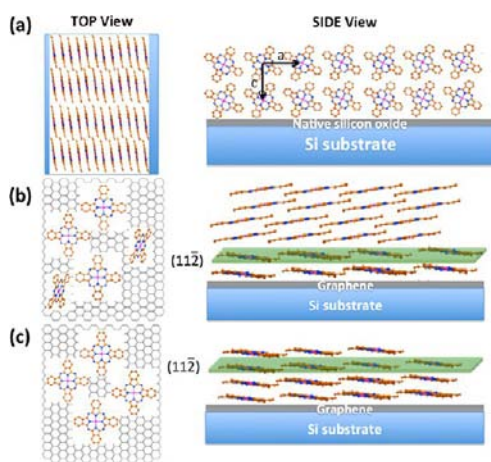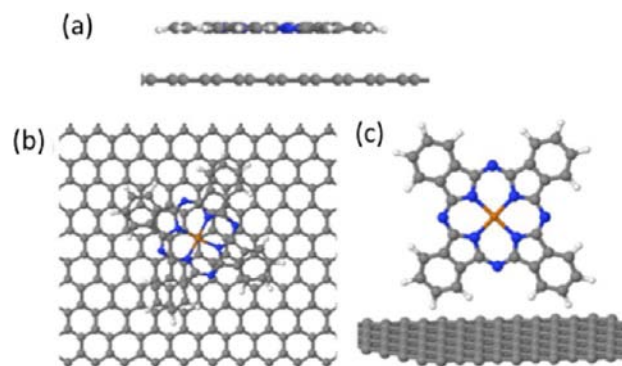
Figure 4. Schematic representations of the possible molecular packing orientations of the CuPc film grown on (a) silicon, (b) graphene at room temperature, and (c) graphene at 130 °C.

Figure 5. (a) Side view of the face-on position, (b) top view of face-on position, and (c) side view of the edge-on position of a CuPc molecule on graphene. The face-on CuPc molecules are strongly bound in both cases. On the other hand, the edge-on position is not stable on graphene, and the initial edge-on position falls back to the face-on position during the structure relaxation processes. Molecules are fully optimized with total energies based on the PBE + vdW correction scheme.[48]

substrate interaction directly affects the molecular electronic coupling with the graphene and the magnitude of the surface dipoles, which are crucial for the energy level alignment at the graphene-organic interfaces and consequently for charge carrier injection in optoelectronic devices. In contrast, the edge-on configuration (Figure 5c) is unstable on graphene, and the starting edge-on position falls back to the more stable face-on (Figure 5a) configuration during the structural relaxation processes. This can be understood from vdW contributions to the binding energy. On graphene vdW interactions are maximized when the π orbitals between the CuPc, and graphene are overlapping (face-on). However, in the edge-on configuration, the orbital overlap is minimized, and vdW interactions are too weak to stabilize that configuration. These theoretical results support the experimental finding that at a low coverage or for thinner films, CuPc molecules prefer a face-on configuration on graphene while the edge-on configuration is energetically unfavorable.

The STM measurements support the theoretical predictions of the orientation of CuPc molecules on graphene in the initial adsorption behavior of CuPc from submonolayer to full coverage. The surface configuration of the CuPc film on graphene, is illustrated by the STM image shown in Figure 6. A
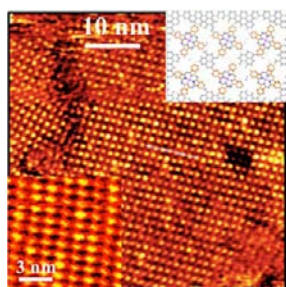

Figure 6. STM image of face-on CuPc molecules on graphene. Bottom-left corner inset is a high-magnification STM image of face-on molecules on graphene. Right inset schematically shows the molecular orientation.

2D ordered structure with 4-fold symmetry was observed. The high-resolution image in a smaller area shows that the two sides of the unit cell are almost perpendicular to each other and exhibit almost the same length value of 1.38 nm. The

observation indicates that the CuPc molecule adopts a flat configuration with the π-plane parallel to the graphene surface.

Figure 7 depicts the evolution of CuPc film morphology on graphene at room temperature and 130 °C with increasing film thickness, in comparison with that on native oxide of Si. CuPc molecules at room temperature begin to preferentially nucleate at wrinkles or at grain boundaries of graphene at low coverage (2 nm) to form small CuPc crystallites, finally forming a continuous film (20 nm) with a well-defined grain boundary by edge growth. The nucleation of other organic molecules at wrinkles in the graphene has also been observed before.[28] CuPc molecules at high temperature also prefer to reside along the wrinkles and the edges of graphene at the initial stage of growth (2 nm coverage) but form 300 nm islands having regular shapes with sharp domain edges. A higher diffusion rate will reduce the nucleation density on the graphene, and nucleation will preferentially occur close to the wrinkles. With increasing coverage on graphene, as expected, higher growth temperature and the resulting enhanced mobility of CuPc molecules on graphene leads to preferential face-to-face column growth of fewer, but larger 2D strip-like crystals aligned along the graphene lattice and grain boundary (see Figure S1) with ordered superstructures that maintained the face-on orientation throughout the growth process. Thicker films at higher (50 nm) coverage formed at high temperature also exhibit extremely large, monocrystalline grains in excess of 1 μm long and 200 nm high (also see Figures 8a and S1) which may potentially enable bulk-like properties for thin films. This presents the basis for growing films with excellent crystalline properties and the potential for a significant improvement of those device properties which are limited by grain size effects and grain boundaries (for example, charge carrier mobility). In contrast, on a silicon substrate (Figure 7e), the CuPc molecules formed homogeneous, continuous small spherical crystallites in a 20 nm thick film at room temperature. At the growth temperature of 130 °C, the CuPc molecules formed elongated crystallites with well-defined grain boundaries on silicon substrates (Figure 7j).

An interesting phenomenon observed in the AFM and SEM images (Figure 8) for CuPc films on graphene at high temperature is that ordered CuPc islands prefer to form on SLG rather than FLG, even at high coverage. In contrast, at room temperature there is no selective growth for the CuPc molecules to form continuous films on both SLG and FLG at
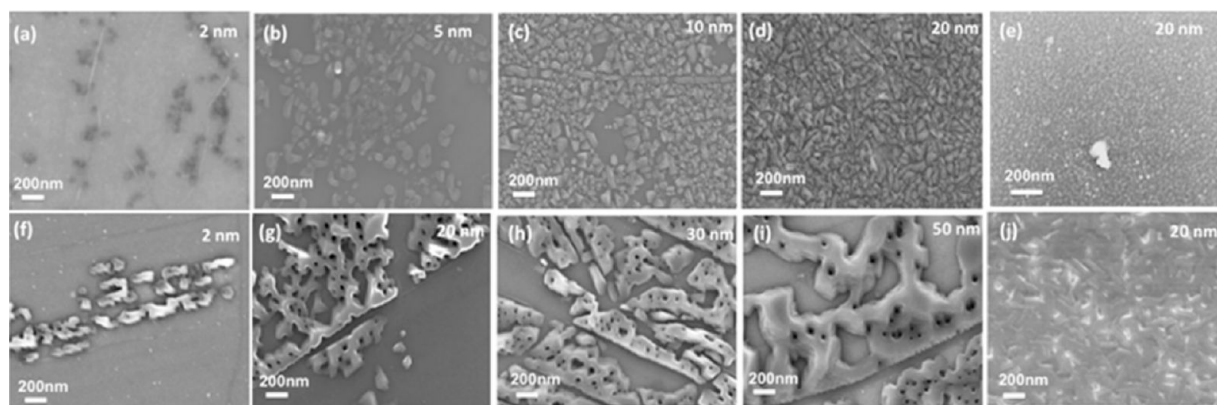

Figure 7. Morphology probed by SEM for CuPc films deposited at room temperature (top row) with thickness (a) 2, (b) 5, (c) 10, (d) 20 nm, on graphene, and (e) 20 nm on a silicon substrate; and at 130 °C (bottom row) with thickness (f) 2, (g) 20, (h) 30, (i) 50 nm on graphene, and (j) 20 nm on a silicon substrate. The dark areas in the SEM images are the voids formed in CuPc crystals while growing on graphene at high temperature.
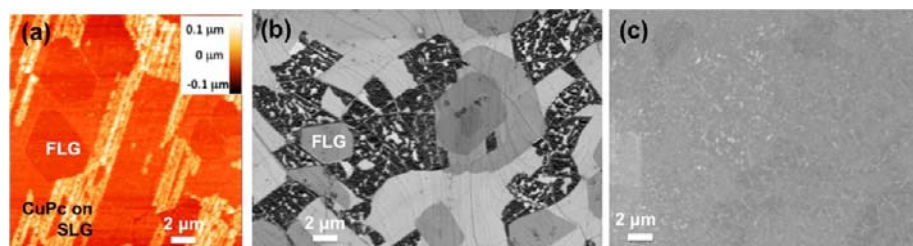
Figure 8. (a) AFM and (b) SEM images of 20 nm CuPc deposited on graphene at 130 °C. CuPc molecules selectively grow on single layer graphene (SLG). At high temperature, no growth was observed on few-layer graphene (FLG). (c) SEM image of 20 nm CuPc deposited on graphene at room temperature. No selective growth of CuPc on SLG.

high coverage, indicating that the film morphology and CuPc grain size are not influenced by the number of graphene layers. Wang et al.[27,43] also observed the similar phenomenon that at room temperatures $CuPcF_{16}$ molecules form a fully covered film on both SLG and FLG at high coverage, but at low coverage the CuPc molecules selectively adsorb on SLG, resulting from a subtle difference in their electronic structures. Such charge-transfer-induced long-rang ordering might have significant effects on the subsequent growth and structure of the organic film and, therefore, on device performance.

The growth mechanism of CuPc on graphene, and more specifically the development of in-plane orientation, are proposed on the basis of our experiments and first-principle calculations. A diffusion barrier of 0.16 eV for CuPc on graphene has been reported.[27,44] The barrier is small enough for CuPc molecules to diffuse freely on graphene to find the most stable adsorption site at low coverage and room temperature. It is known that defects (grain boundaries, vacancies, topological) in graphene promote enhanced binding energies of metal nanoparticles. Therefore, it follows that the CuPc molecules prefer to nucleate close to the wrinkles/defects of the graphene then eventually diffuse to different locations randomly on graphene, as shown in Figure 7. In thermal equilibrium, CuPc molecules on graphene therefore would be expected to lie down to form the energetically most favorable configuration because of the interfacial dipole interaction induced by the charge transfer between the molecules and graphene. Finally, CuPc forms a continuous film with a well-defined grain boundary by edge growth due to the diffusion limitation. According to a previous report, the adsorption energy and the lateral corrugation barrier for CuPc on a graphene surface is very small, and the interaction between the stacking CuPc molecules is much weaker than the CuPc-to-graphene attraction[27,43,44] At high growth temperatures, impinging CuPc molecules have a larger diffusion length and a higher diffusion rate on graphene that will reduce the nucleation density and induce it to preferentially occur on wrinkles and defects. The thermal motion of the deposited CuPc molecules is large. Thus, the resultant large surface migration of the molecules and the small lateral corrugation barrier (lower than the thermal energy) will cause a preference toward island growth. The face-to-face π-stacking of the molecules leads to the formation of molecular columns and a constant molecular orientation parallel to the substrate during the growth. Such an order is maintained by intermolecular van der Waals interactions and the molecule–substrate interaction associated with a small amount of charge transfer from graphene to the CuPc molecule.

CONCLUSION

In summary, graphene is an effective template to nucleate, orient, and pack CuPc molecules in a face-on orientation, which is the ideal structure for high-performance OPVs. In contrast, CuPc assembly on silicon substrates is fundamentally different, with the molecular orientation of CuPc in an edge-on orientation. However, the nucleation and orientation of CuPc molecules on graphene is shown to depend on the growth temperature and thickness, with films grown at room temperature maintaining their face-on orientation only for limited thicknesses while films grown at higher temperatures form face-on orientations throughout the growth process, enabling the synthesis of micrometers-size, strip-like CuPc crystals. The face-on orientation was shown to persist through 50 nm in CuPc film thickness. CuPc molecules at high temperature were shown to preferentially grow on single-layer graphene compared to few-layer graphene, even at high coverage, which was explained on the basis of charge transfer with the substrate and induced interfacial dipole interactions. The demonstrated ability of graphene to template the creation of crystalline, aligned molecular superstructures should permit the design of well-defined model systems to explore nano-structured heterojunctions of electron donors and acceptors. The extremely large, monocrystalline CuPc grains oriented by graphene appear promising as a basis for the growth of thin films with high crystallinity, long-range order, and minimized grain boundaries for enhanced charge transport and exciton transport in organic electronics. This experimental and theoretical investigation indicates the important role that substrates can contribute to tune organic molecular epitaxy for the control of thin film properties.

EXPERIMENTAL SECTION

Sample Preparation and Morphology Characterization.
Graphene grown on a Cu foil or e-beam evaporated 300 nm thick Ni films was covered with polymethylmethacrylate (PMMA) and floated in an aqueous solution of 1 M $FeCl_3$. After copper layers were etched away, the graphene film with PMMA support was transferred to a target substrate. The graphene film remained on the substrate after removal of the PMMA support with acetone. Thermal treatment of the sample at temperatures (~500 °C) to decompose any residual PMMA was found to be an effective way to remove these residues. The details of CVD growth and graphene transfer are described elsewhere.[45]

CuPc was thermally evaporated on Si wafers with native oxide layer and on graphene substrates under a pressure of $<10^{-7}$ Torr using Angstron Engineering chambers. The substrate was held at room temperature or 130 °C and a nominal growth rate of 0.05 nm/s was used, as monitored with a quartz microbalance.

The surface morphologies of the CuPc films were observed on Asylum AFM and Zeiss Merlin VP SEM/STEM.

X-ray Measurements. The X-ray diffraction measurements were performed ex-situ on a Philips X'Pert diffractometer equipped with an ATC3 texture cradle and a flat graphite monochromator. The system was operated with Cu Kα radiation with point focus. A wide open slit geometry and a short beam path length were used to optimize the sensitivity of the system. In specular scans the scattering vector **q** runs along the z-direction, $\mathbf{q}_z$, and net planes are detected which lie parallel to the sample surface. A phase analysis and out-of-plane orientations of the crystallites are thus obtained. To verify the in-plane alignment of the CuPc crystals, pole figures were measured. Since a pole figure is measured at constant |**q**|, one gets a spatial distribution of a certain net plane relative to the surface of the sample. The direction of scattering vectors in pole figures were compared with stereograms and calculated on the basis of single-crystal data. 2D GIXS data were collected using an Anton Paar SAXSess mc^2 spectrometer (high-resolution grazing incidence scattering with a point X-ray beam). The detector was positioned about 270 mm from the sample. The camera length was calibrated using a silver behenate as a standard with known lattice spacing. The incident angle was 0.2°. The scattering spectra were collected as a 2D image map using an image plate that was divided into a component in the plane of the substrate and a component perpendicular to the substrate.

STM. STM measurement was performed using a Omicron/Nanonis system. To examine the growth process of CuPc on graphene, CuPc molecules were thermally deposited on an epitaxial graphene surface at room temperature. The graphene substrate was grown from a 4H-SiC (0001) wafer on the Si face at 1590 °C for 30 min using solid-state graphitization in an Ar environment. Stable imaging of the molecules on graphene at room temperature was not possible as the molecules were very mobile under the tip during scanning. Cooling the graphene sample to 100 K resulted in stable imaging of the molecular self-assembly.

First-Principles Calculations. We employed a highly accurate, all-electron first-principles quantum mechanical calculation code with numerical atom-centered orbitals as basis set (FHI-aims).[46] The exchange-correlation potential of the Perdew−Burke−Ernzerhof version of the generalized-gradient approximation[47] was used. In addition, nonempirical vdW corrections based on the PBE charge densities[48] were performed to capture the long-range dispersion interactions, which are missing in the conventional exchange-correlation functionals. All the CuPc molecules on the substrates were fully optimized while the substrates keep constrained to the bulk lattice constant. The optimized structures were obtained once the total force is smaller than 0.01 eV/Å. These configurations are constructed within a supercell with a large vacuum size of ∼50 Å, the nearest neighbor CuPc distance is 24.7 Å on graphene, and no k-point sampling was performed (i.e., Γ point calculations). The calculation setup mimics a low coverage of CuPc molecules on graphene, where intermolecular interaction is negligible.

ASSOCIATED CONTENT

Ⓢ Supporting Information
High-resolution SEM images of large crystals of CuPc grown on graphene at high temperatures. This material is available free of charge via the Internet at http://pubs.acs.org.

AUTHOR INFORMATION

Corresponding Author
xiaok@ornl.gov
Notes
The authors declare no competing financial interest.

ACKNOWLEDGMENTS

REFERENCES

(1) Facchetti, A. *Chem. Mater.* **2011**, *23*, 733.
(2) Wang, C. L.; Dong, H. L.; Hu, W. P.; Liu, Y. Q.; Zhu, D. B. *Chem. Rev.* **2012**, *112*, 2208.
(3) Smits, E. C. P.; Mathijssen, S. G. J.; van Hal, P. A.; Setayesh, S.; Geuns, T. C. T.; Mutsaers, K. A. H. A.; Cantatore, E.; Wondergem, H. J.; Werzer, O.; Resel, R.; Kemerink, M.; Kirchmeyer, S.; Muzafarov, A. M.; Ponomarenko, S. A.; de Boer, B.; Blom, P. W. M.; de Leeuw, D. M. *Nature* **2008**, *455*, 956.
(4) Mishra, A.; Bauerle, P. *Angew. Chem. Int. Ed.* **2012**, *51*, 2020.
(5) Dimitrakopoulos, C. D.; Malenfant, P. R. L. *Adv. Mater.* **2002**, *14*, 99.
(6) Wen, Y. G.; Liu, Y. Q.; Guo, Y. L.; Yu, G.; Hu, W. P. *Chem. Rev.* **2011**, *111*, 3358.
(7) Bredas, J. L.; Norton, J. E.; Cornil, J.; Coropceanu, V. *Acc. Chem. Res.* **2009**, *42*, 1691.
(8) Sullivan, P.; Jones, T. S.; Ferguson, A. J.; Heutz, S. *Appl. Phys. Lett.* **2007**, *91*, 233914.
(9) Bartels, L. *Nat. Chem.* **2010**, *2*, 87.
(10) Sykes, E. C. H.; Han, P.; Kandel, S. A.; Kelly, K. F.; McCarty, G. S.; Weiss, P. S. *Acc. Chem. Res.* **2003**, *36*, 945.
(11) Stadler, C.; Hansen, S.; Kroger, I.; Kumpf, C.; Umbach, E. *Nat. Phys.* **2009**, *5*, 153.
(12) Chen, Q.; Rada, T.; McDowall, A.; Richardson, N. V. *Chem. Mater.* **2002**, *14*, 743.
(13) Naito, R.; Toyoshinia, S.; Ohashi, T.; Sakurai, T.; Akimoto, K. *Jpn. J. Appl. Phys.* **2008**, *47*, 1416.
(14) Resel, R.; Ottmar, M.; Hanack, M.; Keckes, J.; Leising, G. *J. Mater. Res.* **2000**, *15*, 934.
(15) Xiao, K.; Liu, Y.; Yu, G.; Zhu, D. *Appl. Phys. A-Mater.* **2003**, *77*, 367.
(16) Zhou, Y.; Taima, T.; Miyadera, T.; Yamanari, T.; Kitamura, M.; Nakatsu, K.; Yoshida, Y. *Nano Lett.* **2012**, *12*, 4146.
(17) Rand, B. P.; Cheyns, D.; Vasseur, K.; Giebink, N. C.; Mothy, S.; Yi, Y. P.; Coropceanu, V.; Beljonne, D.; Cornil, J.; Bredas, J. L.; Genoe, J. *Adv. Funct. Mater.* **2012**, *22*, 2987.
(18) Hong, D.; Do, Y. R.; Kwak, H. T.; Yim, S. *J. Appl. Phys.* **2011**, *109*, 063507.
(19) Yook, K. S.; Chin, B. D.; Lee, J. Y.; Lassiter, B. E.; Forrest, S. R. *Appl. Phys. Lett.* **2011**, *99*, 043308.
(20) Novoselov, K. S.; Geim, A. K.; Morozov, S. V.; Jiang, D.; Zhang, Y.; Dubonos, S. V.; Grigorieva, I. V.; Firsov, A. A. *Science* **2004**, *306*, 666.
(21) Kim, K. S.; Zhao, Y.; Jang, H.; Lee, S. Y.; Kim, J. M.; Kim, K. S.; Ahn, J. H.; Kim, P.; Choi, J. Y.; Hong, B. H. *Nature* **2009**, *457*, 706.
(22) Wan, X. J.; Long, G. K.; Huang, L.; Chen, Y. S. *Adv. Mater.* **2011**, *23*, 5342.
(23) De Arco, L. G.; Zhang, Y.; Schlenker, C. W.; Ryu, K.; Thompson, M. E.; Zhou, C. W. *ACS Nano* **2010**, *4*, 2865.
(24) Liu, Z. F.; Liu, Q.; Huang, Y.; Ma, Y. F.; Yin, S. G.; Zhang, X. Y.; Sun, W.; Chen, Y. S. *Adv. Mater.* **2008**, *20*, 3924.
(25) Sykes, E. C. H. *Nat. Chem.* **2009**, *1*, 175.
(26) Wang, Q. H.; Hersam, M. C. *Nat. Chem.* **2009**, *1*, 206.
(27) Wang, Y. L.; Ren, J.; Song, C. L.; Jiang, Y. P.; Wang, L. L.; He, K.; Chen, X.; Jia, J. F.; Meng, S.; Kaxiras, E.; Xue, Q. K.; Ma, X. C. *Phys. Rev. B* **2010**, *82*, 245420.
(28) Hlawacek, G.; Khokhar, F. S.; van Gastel, R.; Poelsema, B.; Teichert, C. *Nano Lett.* **2011**, *11*, 333.
(29) Hlawacek, G.; Khokar, F. S.; van Gastel, R.; Teichert, C.; Poelsema, B. *IBM J. Res. Dev.* **2011**, *55*, 15.

(30) Lee, W. H.; Park, J.; Sim, S. H.; Lim, S.; Kim, K. S.; Hong, B. H.; Cho, K. *J. Am. Chem. Soc.* **2011**, *133*, 4447.

(31) Colson, J. W.; Woll, A. R.; Mukherjee, A.; Levendorf, M. P.; Spitler, E. L.; Shields, V. B.; Spencer, M. G.; Park, J.; Dichtel, W. R. *Science* **2011**, *332*, 228.

(32) Xiao, K.; Liu, Y.; Guo, Y.; Yu, G.; Wan, L.; Zhu, D. *Appl. Phys. A-Mater.* **2005**, *80*, 1541.

(33) Yang, F.; Shtein, M.; Forrest, S. R. *Nat. Mater.* **2005**, *4*, 37.

(34) Peisert, H.; Schwieger, T.; Auerhammer, J. M.; Knupfer, M.; Golden, M. S.; Fink, J.; Bressler, P. R.; Mast, M. *J. Appl. Phys.* **2001**, *90*, 466.

(35) Vergnat, C.; Landais, V.; Legrand, J. F.; Brinkmann, M. *Macromolecules* **2011**, *44*, 3817.

(36) Wang, S. D.; Dong, X.; Lee, C. S.; Lee, S. T. *J. Phys. Chem. B* **2004**, *108*, 1529.

(37) Mao, J. H.; Zhang, H. G.; Jiang, Y. H.; Pan, Y.; Gao, M.; Xiao, W. D.; Gao, H. J. *J. Am. Chem. Soc.* **2009**, *131*, 14136.

(38) Dou, W. D.; Huang, S. P.; Zhang, R. Q.; Lee, C. S. *J. Chem. Phys.* **2011**, *134*, 094705.

(39) Hoshino, A.; Takenaka, Y.; Miyaji, H. *Acta Crystallogr. B* **2003**, *59*, 393.

(40) Dresselhaus, M. S.; Dresselhaus, G. *Adv. Phys.* **2002**, *51*, 1.

(41) Cruickshank, A. C.; Dotzler, C. J.; Din, S.; Heutz, S.; Toney, M. F.; Ryan, M. P. *J. Am. Chem. Soc.* **2012**, *134*, 14302.

(42) Kim, H. J.; Lee, H. H.; Kim, J. W.; Jang, J.; Kim, J. J. *J. Mater. Chem.* **2012**, *22*, 8881.

(43) Ren, J.; Meng, S.; Wang, Y. L.; Ma, X. C.; Xue, Q. K.; Kaxiras, E. *J. Chem. Phys.* **2011**, *134*, 194706.

(44) Yin, S. X.; Wang, C.; Xu, B.; Bai, C. L. *J. Phys. Chem. B* **2002**, *106*, 9044.

(45) Vlassiouk, I.; Regmi, M.; Fulvio, P. F.; Dai, S.; Datskos, P.; Eres, G.; Smirnov, S. *ACS Nano* **2011**, *5*, 6069.

(46) Blum, V.; Gehrke, R.; Hanke, F.; Havu, P.; Havu, V.; Ren, X.; Reuter, K.; Scheffler, M. *Comput. Phys. Commun.* **2009**, *180*, 2175.

(47) Perdew, J. P.; Burke, K.; Ernzerhof, M. *Phys. Rev. Lett.* **1996**, *77*, 3865. Perdew, J. P.; Burke, K.; Ernzerhof, M. *Phys. Rev. Lett.* **1997**, *78*, 1396.

(48) Tkatchenko, A.; Scheffler, M. *Phys. Rev. Lett.* **2009**, *102*, 073005.